Spatial and Diurnal Variations of Aerosol Organosulfates in Summertime Shanghai, China: Potential Influence of Photochemical Process and Anthropogenic Sulfate Pollution

Ting Yang[1], Yu Xu[1,*], Qing Ye[1], Yi-Jia Ma[1], Yu-Chen Wang[2], Jian-Zhen Yu[2], Yu-Sen Duan[3], Chen-Xi Li[1], Hong-Wei Xiao[1], Zi-Yue Li[1], Yue Zhao[1,*], Hua-Yun Xiao[1,*]

[1]School of Environmental Science and Engineering, Shanghai Jiao Tong University, Shanghai 200240, China

[2]Division of Environment & Sustainability, Hong Kong University of Science & Technology, Hong Kong SAR, China

[3]Shanghai Environmental Monitoring Center, Shanghai 200235, China

*Corresponding authors

Yu Xu, e-mail: xuyu360@sjtu.edu.cn

Yue Zhao, e-mail: yuezhao20@sjtu.edu.cn

Hua-Yun Xiao, e-mail: xiaohuayun@sjtu.edu.cn

ABSTRACT：Organosulfates (OSs) are ubiquitous aerosol components with intense research over years. However, spatial and diurnal variations in OS formation in polluted atmospheres remain poorly understood. In this study, 130 OS species were quantified (or semi-quantified) in ambient fine particulate matter ($PM_{2.5}$) collected in urban and suburban Shanghai (East China) in summer 2021. Isoprene- and monoterpene-derived OSs were dominant OS groups (averaging 51% and 19% of total quantified OSs, respectively), likely indicating a large biogenic contribution to OS formation in summer. Most OSs peaked during daytime, while monoterpene-derived nitrooxy-OSs (NOS_m) increased during nighttime. Accordingly, OSs were largely produced via daytime formation processes, rather than nighttime chemistry, except for NOS_m. Additionally, although OS formation in the urban and suburban areas exhibited similar diurnal variations, the average concentrations of biogenic and anthropogenic OSs decreased significantly from the urban site to the suburban site. Furthermore, we concretized daytime OS formation based on the interactions among OSs, ultraviolet (UV), ozone (O_3), and sulfate (SO_4^{2-}). Indeed, the concentrations of most OSs were significantly correlated with the values of $UV[O_3][SO_4^{2-}]$ during daytime in both urban and suburban Shanghai. In particular, the correlation between major OSs and $UV[O_3][SO_4^{2-}]$ was stronger than the correlation of major OSs with O_3 and SO_4^{2-}; moreover, there was no significant correlation between major OSs and UV. Thus, higher urban OS events were attributed to the enhanced photochemical processes and sulfate level in the urban area. Overall, this study provides field evidence for the influence of photochemical processes and anthropogenic sulfate on OS formation and has important implications for the

47   mitigation of organic particulate pollution.

48   **KEYWORDS:** Organosulfates; Aerosols; Photooxidation; Sulfate pollution; Shanghai

49

1. Introduction

51   Organosulfates (OSs) are ubiquitous constituents in secondary organic aerosol

52   (SOA) and can contribute up to ~30% of organic mass in atmospheric fine particles

53   ($PM_{2.5}$) (Tolocka andTurpin 2012; Surratt et al. 2008; Hettiyadura et al. 2018). OSs

54   affect the formation, hygroscopicity, light-absorbing property, and acidity of organic

55   aerosols as well as biogeochemical cycles of sulfur (Estillore et al. 2016; Riva et al.

56   2019; Fleming et al. 2019), which are tightly associated with air quality, human health,

57   and regional climate (Ramanathan et al. 2001; Menon et al. 2008). Thus, understanding

58   the mechanisms and key influencing factors of OS formation in the ambient atmosphere

59   is of great significance for an effective assessment of environment and climate effects

60   of OSs.

61   Many laboratory studies have suggested that heterogeneous and multiphase

62   reactions involving biogenic and anthropogenic volatile organic compounds (VOCs),

63   their oxidation intermediates, and sulfate or gas-phase sulfur dioxide (SO_2) are

64   important pathways for the formation of OSs (Blair et al. 2017; Riva et al. 2016b; Ye et

65   al. 2018). For example, the formation of 2-methyltetrol sulfate ester (2-MT-OS) and 2-

66   methylglyceric acid sulfate ester (2-MGA-OS) can be attributed to the reactive uptake

67   of isoprene epoxydiols (IEPOX) and isoprene-derived hydroxymethyl-methyl-α-

68   lactone (HMML) by acidic particles, respectively (Surratt et al. 2010; Nguyen et al.

2015). The ozonolysis of α-pinene and limonene in the presence of SO_2 can contribute

to the production of monoterpene-derived OSs (e.g., $C_9H_{15}O_7S^-$ and $C_{10}H_{17}O_7S^-$) (Ye

et al. 2018). Chamber experiments by Riva et al. (2016b) showed that the

photooxidation of C_{10}–C_{12} alkanes is associated with the formation of aliphatic OSs.

More recently, the aliphatic OSs have been identified based on the uptake experiments

of SO_2 by oleic acid and other unsaturated fatty acids (Shang et al. 2016; Passananti et

al. 2016). In addition, the gas-phase oxidation of polycyclic aromatic hydrocarbons was

found to be an important source of aromatic OSs (Riva et al. 2015).

Furthermore, OSs have been identified in different ambient atmospheres, including

suburban (Surratt et al. 2007b), rural (Hettiyadura et al. 2017; Hettiyadura et al. 2018;

Budisulistiorini et al. 2015), urban (Kanellopoulos et al. 2022; Stone et al. 2012; Surratt

et al. 2007b), marine (Hawkins et al. 2010), polar (Hansen et al. 2014), and forest areas

(Iinuma et al. 2007). In particular, Chen et al. (2021) investigated aerosol OSs across

the Interagency Monitoring of Protected Visual Environments (IMPROVE) network of

the U.S. (20 sites). Owing to different levels of precursors and atmospheric pollution,

the abundance and formation pathways of OSs change substantially in temporal and

spatial scales (Wang et al. 2021; Ding et al. 2022; Jiang et al. 2022; Nozière et al. 2010;

O'brien et al. 2014). Patently, field observations are valuable for verifying the

mechanistic understanding of OS formation obtained in the laboratory studies. The

importance of atmospheric oxidants and sulfate (or SO_2) in the OS formation was

proposed in field observations according to a correlation analysis of OSs with ozone

(O_3) (or the sum of O_3 and NO_2 concentrations) and sulfate (or SO_2) (Nguyen et al.

91   2014; Hettiyadura et al. 2019; Wang et al. 2018). Notably, these observation-based

92   studies also highlighted the role of photochemistry of OS precursors. However, the

93   interactions among ultraviolet (UV), O_3, and sulfate have not been well investigated. In

94   particular, few studies were performed to systematically reveal the difference in the

95   formation processes of OSs in polluted and clean areas, as well as during daytime and

96   nighttime.

97   Shanghai is a megacity in the Yangtze River Delta (YRD) region of China.

98   Locally varied ambient conditions such as O_3, SO_2, and NO_x, relative humidity (RH),

99   and aerosol acidity affect the formation of OSs significantly (Cai et al. 2020; Wang et

100   al. 2021). Here, 130 OS species were quantified (or semi-quantified) in $PM_{2.5}$ samples

101   collected in urban and suburban Shanghai in summer 2021 to investigate the relative

102   influence of photochemistry and nighttime chemistry on OS formation and their

103   linkages with anthropogenic sulfate pollution. In addition, the potential impacts of

104   aerosol acidity and aerosol liquid water (ALW) on OS formation were discussed. This

105   study can help to deepen the understanding of photochemical process and nighttime

106   chemistry of OSs in the atmosphere.

107

108   **2. Materials and Methods**

109   **2.1 Site Description and Sample Collection**

110   Ambient $PM_{2.5}$ samples were continuously collected in the urban center and

111   suburban area in Shanghai from 11 to 23 July 2021 (**Figure S1**). The sampling site in

112   the urban center is located on the roof of a building (~20 m above the ground) in the

Xuhui Campus of Shanghai Jiao Tong University. The site is characterized by a typical

urban environment with heavy traffic and dense population (~1.12 million people in

Xuhui district). The aerosol sampler in the suburban area was placed on the roof of a

~20 m high building in a monitoring station of Pudong Huinan. This site is closer to the

coastline than the urban sampling site (**Figure S1**). Thus, the suburban site is expected

to be more affected by clean air mass from the sea. $PM_{2.5}$ was sampled onto the

prebaked (550°C for ~8 h) quartz fiber filters (8 × 10 in., Whatman) using a high-

volume air sampler (HiVol 3000, Ecotech) at a flow rate of 67.8 m^3 min^{-1}. The duration

of each sample collection in both urban and suburban areas was approximately 11 h

during the daytime (8:30−19:30 LT) and 12 h during the nighttime (20:00−8:00 LT).

Two blank filter samples were collected at each site during the campaign. A total of 50

filter samples were collected, which were stored at −30°C until analysis. It should be

pointed out that the concentrations of detected OSs could be impacted by the sampling

process without denuding SO_2 (Kristensen et al. 2016; Brüggemann et al. 2021).

However, if SO_2 can heterogeneously react with organic species on filters to form OSs,

these processes should also occur on ambient particle matter before the sample was

collected. Thus, we did not consider the potential impact of $PM_{2.5}$ collection without

denuding SO_2 on OS measurements in this study. In the future, the relative importance

of the heterogeneous sulfation reactions on filter and ambient particle matter should be

further evaluated for different environments.

2.2 Chemical Analysis and Prediction of Aerosol Acidity and ALW

135   A portion of the filter (~15.9 cm^2) was extracted with 3 mL methanol in an

136   ultrasonic bath for 30 min for two times. The sodium camphor sulfonate (1 ppm) was

137   spiked on the filter punches as an internal standard before extracting. The extracts

138   obtained each time were combined and filtered through a 0.22 μm Teflon syringe filter

139   (CNW Technologies GmbH) and then concentrated to 300 μL under a gentle stream of

140   ultra-high-purity nitrogen gas. Subsequently, 300 μL ultrapure water was added into the

141   concentrated samples, followed by centrifugation to get the supernatant for analysis.

142   OSs were analyzed using an Acquity UPLC (Waters, USA) coupled to a Xevo G2-XS

143   Quadrupole time-of-flight mass spectrometer (ToF-MS, Waters, USA) equipped with

144   an electrospray ionization (ESI) source operated in the negative ion mode. The

145   chromatographic conditions and analytical procedures were detailed in our recent

146   publication (Wang et al. 2021).

147   A total of 212 OSs were identified by UPLC-MS analysis, in which 130 OS species

148   were quantified (or semi-quantified) (**Table 1** and **Table S1**). The quantified (or semi-

149   quantified) species included isoprene-derived OSs (OS$_i$), monoterpene-derived OSs

150   (OS$_m$), C$_2$-C$_3$ OSs, aliphatic OSs, and aromatic OSs (Hettiyadura et al. 2019). It is worth

151   noting that most of identified OSs were semi-quantified using surrogate standards

152   because of the lack of authentic standards (Staudt et al. 2014; Hettiyadura et al. 2015).

153   The surrogate OS standards included potassium phenyl sulfate (98%, Tokyo Chemical

154   Industry), methyl sulfate (99%, Macklin), sodium octyl sulfate (95%, Sigma-Aldrich),

155   glycolic acid sulfate (artificial synthesis), lactic acid sulfate (artificial synthesis),

156   limonaketone sulfate (artificial synthesis), and α-pinene sulfate (artificial synthesis)

157 (Olson et al. 2011; Wang et al. 2017; Hettiyadura et al. 2019; Hettiyadura et al. 2017;

158 Wang et al. 2018), as detailed by our previous study (Wang et al. 2021). Considering

159 that OSs with similar structures of carbon backbone typically have similar MS

160 responses (Wang et al. 2021; Wang et al. 2017), the selection of surrogate standard for

161 a given OS was primarily based on the similarities in the carbon chain structure of the

162 standard and targeted OS species (Hettiyadura et al. 2017). Furthermore, the similarities

163 of the sulfur-containing fragment ions in the MS/MS spectra of the standard and

164 targeted OS species have also been adopted (Wang et al. 2021; Hettiyadura et al. 2019).

165 For OSs that have been reported in previous studies, MS/MS can further support their

166 structural identifications (**Table 1**). However, most of OSs without identified structural

167 information were classified and semi-quantified according to their molecular formulas

168 and correlation analysis with known OSs and unidentified OSs (**Sect. S1**) (Bryant et al.

169 2021; Hettiyadura et al. 2019). Details about the standards used for quantitative OS

170 species as well as about the classification or identification of OSs were shown in Table

171 1, Table S1, and Supplementary Information (**Sect. S1**). We found that most of OSs

172 without identified structural information in previous studies and this study had

173 significantly lower peak intensity compared to those listed in Table 1, implying that

174 these OS compounds have weak impact on total OS abundance in ambient aerosols. In

175 general, the differential ionization efficiencies and fragmentation patterns in the OS

176 measurement may introduce biases (Hettiyadura et al. 2017). Consequently, the OS

177 species shown in Table 1 and Table S1 should not be regarded as an accurate measure

178 of OS compounds, but a best solution in the absence of authentic OS standards

179   (Hettiyadura et al. 2015; Hettiyadura et al. 2017; Hettiyadura et al. 2019; Wang et al.

180   2021). The recoveries of OS standards ranged from 84% to 94% (87%±4%). Thus, we

181   assumed that there is a high extraction efficiency for major OS species in this study, as

182   indicated by previous studies (Wang et al. 2021; Hettiyadura et al. 2015). Detailed data

183   quality control was described in our recent publication (Wang et al. 2021).

184   The mass concentrations of organic carbon (OC) and elemental carbon (EC) were

185   determined via an OC/EC analyzer (DRI Model 2015). The mass concentrations of OC

186   were converted to those of organic matter (OM) using a conversion factor of 1.6 (Turpin

187   andLim 2001; Wang et al. 2021; Wang et al. 2018). The mass concentrations of

188   inorganic ions in $PM_{2.5}$ samples, including Na^+, NH_4^+, K^+, Mg^{2+}, Ca^{2+}, Cl^-, NO_3^-, and

189   SO_4^{2-}, were measured using an ion chromatograph system (ICS-5000+, Thermo, USA).

190   A thermodynamic model (ISORROPIA-II) was used to predict the mass

191   concentration of ALW and pH (Guo et al. 2015; Hennigan et al. 2015). The model was

192   operated with particle-phase concentrations of Na^+, SO_4^{2-}, NH_4^+, NO_3^-, Cl^-, Ca^{2+}, K^+,

193   and Mg^{2+}, as well as ambient temperature (T) and RH as the inputs. Moreover, the

194   forward mode with the thermodynamically metastable state was selected. The detailed

195   descriptions on ALW and pH predictions were shown in our previous studies (Wang et

196   al. 2021; Xu et al. 2020). In particular, we compared different outputs of the pH values

197   calculated by ISORROPIA-II between the cases with and without considering OSs as

198   additional sulfates to investigate potential impact of OSs on pH prediction (Riva et al.

199   2019). The pH values predicted from these two cases (2.55 ± 0.93 vs 2.65 ± 0.94 at the

200   urban site and 2.17 ± 0.68 vs 2.23 ± 0.74 at the suburban site) have an insignificant

201 difference. Thus, OSs were expected to have a considerably small contribution to pH

202 prediction in this study.

203

204 **2.3. Auxiliary Data and Data Analysis**

205 The transport trajectories of air masses arriving at the sampling sites during the

206 sampling period were created using the database of NOAA's Air Resources Laboratory

207 (NOAA's Air Resources Laboratory, USA) and MeteoInfoMap software coupled with

208 TrajStat program (Chinese Academy of Meteorological Sciences, China). The data of

209 T, RH, wind speed, and UV irradiation as well as the concentrations of NO, NO_2, O_3,

210 SO_2, and $PM_{2.5}$ at the urban and suburban sites were obtained from the environmental

211 monitoring stations of Xuhui (~4 km away from the sampling site) and Pudong Huinan

212 (~10 m away from the sampling site), respectively. The ventilation coefficient (VC) can

213 be used to characterize the state of atmospheric dilution in pollutant concentrations

214 (Gani et al. 2019). The VC value can be expressed as a product of wind speed and

215 planetary boundary layer height (PBLH).

216

217 **3. Results and Discussion**

218 **3.1. Molecular compositions and concentrations of OSs**

219 The mass concentrations and mass fractions of the OS species in $PM_{2.5}$ collected

220 in Shanghai were shown in **Figure 1**, with a focus on their spatial and diurnal

221 differences. On average, isoprene-derived OSs (i.e., OS_i) were the dominant

222 components at both urban and suburban sites (**Figures 1a,d**), which accounted for 53.9

± 0.1% and 48.1 ± 0.1% of the total OS masses, respectively. The mass fractions and concentrations of $C_5H_{11}O_7S^-$ were the highest among all kinds of OS_i. In contrast, OS_i containing nitrogen atoms only accounted for a small proportion of OS_i in both urban and suburban areas (**Figures 1a,d** and **Table S2**). Monoterpene-derived OSs (OS_m) were the second most abundant OS components, whose concentrations averaged 30.6 ± 46.4 ng m^{-3} and 19.3 ± 25.7 ng m^{-3} in the urban and suburban areas, respectively. Moreover, the abundance of OS_m was also less controlled by nitrogen-containing OS_m. On average, the OS species with two or three carbon atoms (C_2-C_3 OSs) and anthropogenic OSs (OS_a) together contributed to 26.8% and 33.1% of total OS concentrations in the urban and suburban areas, respectively (**Figures 1a,d** and **Table S3**). A similar pattern in the relative abundance of different groups of OSs was also observed at the same sites in summer 2020 (**Figure S2**). The predominance of OS_i was well documented by many previous observations in Beijing, China (Wang et al. 2018), Guangzhou, China (Bryant et al. 2021), and Atlanta, Georgia, USA (Hettiyadura et al. 2019), Hong Kong, China (Wang et al. 2022), Copenhagen, Denmark (Nguyen et al. 2014), Centreville, AL, USA (Hettiyadura et al. 2017), Zion, Illinois, USA (Hughes et al. 2021), Birmingham, Alabama, USA (Rattanavaraha et al. 2016), Yorkville, GA, USA (Lin et al. 2013), Look Rock, TN, USA (Budisulistiorini et al. 2015). A reasonable explanation for these cases is that there is a large biogenic emission of isoprene, particularly during summer days with higher temperature than in other seasons (Bryant et al. 2021). Interestingly, we found that the mass concentrations of all types of OSs (i.e., total OS_i, OS_m, C_2-C_3 OSs, and OS_a) tended to decrease from the urban area to the

11

245   suburban area. This spatial difference in OS concentrations can be attributed to varied

246   atmospheric oxidation capacity and aerosol properties (e.g., sulfate, acidity, and ALW)

247   (Wang et al. 2021), which will be discussed in detail below.

248   **Table S4** gives an overview of OSs in $PM_{2.5}$ in different regions around the world.

249   The concentrations of total OSs in our study (more than 102.3 ng m^{-3}) were higher than

250   those in Copenhagen, Denmark (59.0 ng m^{-3}) (Nguyen et al. 2014), and Beijing, China

251   (48.7 ng m^{-3}) (Wang et al. 2018). However, the OSs showed a lower concentration in

252   Shanghai compared to the observations in Guangzhou (486.4 ng m^{-3}) (Wang et al. 2022)

253   and Atlanta, USA (Hettiyadura et al. 2019) (1249.4 ng m^{-3}). The concentrations of OS_i

254   in this study were lower than those observed in summertime Atlanta, USA (1123.0 ng

255   m^{-3}) (Hettiyadura et al. 2019), Guangzhou, China (460.2 ng m^{-3}) (Wang et al. 2022),

256   and Hongkong, China (163.2 ng m^{-3}) (Wang et al. 2022), Yorkville, GA, USA (115.11

257   ng m^{-3}) (Lin et al. 2013), Look Rock, TN, USA (180.90 ng m^{-3}) (Budisulistiorini et al.

258   2015), Birmingham, Alabama, USA (176.30 ng m^{-3}) (Rattanavaraha et al. 2016),

259   Manaus, Brazil (390.00 ng m^{-3}) (Cui et al. 2018), but higher than Copenhagen,

260   Denmark (11.3 ng m^{-3}) (Nguyen et al. 2014), Seashore, CA, USA (22.00 ng m^{-3}) (Chen

261   et al. 2021), National Park, CO, USA (19.00 ng m^{-3}) (Chen et al. 2021), National

262   Monument, AZ, USA (3.00 ng m^{-3}) (Chen et al. 2021). For OS_m and C_2-C_3 OSs, their

263   concentrations also showed a variable range in different regions (**Table S4**). The

264   concentrations of OS_a in this study were much higher than those in previous

265   observations (Hettiyadura et al. 2017; Kanellopoulos et al. 2022), which is likely

266   explained by more OS_a species being quantified or higher air pollution level in this study.

267 It should be noted that these spatial comparisons for OS levels mentioned above

268 involved more or less uncertainty due to the lack of authentic standards for precise

269 quantification of OSs. However, our semi-quantitative data provides at least literature

270 reference for future research on these OSs. At the same study site, the abundances of

271 biogenic OSs (OS_i + OS_m) were typically higher than those of other types of OSs,

272 particularly during the summertime when vegetation grows vigorously (**Table S4**).

273 Thus, the yield of summertime OSs in the investigated areas largely depends on the

274 emission level of biogenic VOCs and the air pollution status.

275 We found that the contributions of total OSs to OM were $1.3 \pm 0.5\%$ and $1.9 \pm 0.5\%$

276 at urban and suburban sites in summer 2021, respectively, which were similar to the

277 cases observed in Birmingham, Alabama, USA (1.7%) (Rattanavaraha et al. 2016) and

278 Manaus, Brazil (1.3%) (Cui et al. 2018). These proportions of total OSs in OM were

279 larger than those observed in Beijing, China (0.3%) (Wang et al. 2018) and Centreville,

280 USA (0.2%) (Hettiyadura et al. 2017). However, significant higher contribution of total

281 OSs to OM was observed in Look Rock, TN, USA (36.3%) (Budisulistiorini et al. 2015),

282 Great Smoky Mountains National Park, TN, USA (7.0%) (Chen et al. 2021), Shining

283 Rock Wilderness, NC , USA (5.0%) (Chen et al. 2021), Bondville, IL, USA (6.2%)

284 (Chen et al. 2021), and Atlanta, USA (10.3%) (Hettiyadura et al. 2019) where the

285 formation of OSs was largely impacted by the oxidation of biogenic VOCs. In particular,

286 total OSs contributed to $1.2 \pm 0.8\%$ of OM in summer 2015 and $1.1 \pm 0.8\%$ of OM in

287 summer 2019 in urban Shanghai (Wang et al. 2021). Thus, although anthropogenic

288 emission reduction has been vigorously promoted by the local government in recent

289 years (Guo et al. 2022; Pei et al. 2022) , the contribution of SOA to OM in Shanghai

290 has not decreased significantly as expected (Wang et al. 2021).

291 **Figures 1b,e** show diurnal differences in the mass concentrations and mass

292 fractions of the OS components in $PM_{2.5}$ collected at the urban site. The OS_i was the

293 dominant sulfur-containing species regardless of in daytime and nighttime. However,

294 the concentrations of OS_i exhibited a significant decrease from the daytime (117.8 $\pm$

295 148.1 ng m^{-3}) to the nighttime (43.9 $\pm$ 62.0 ng m^{-3}), except for isoprene-derived

296 nitrooxyorganosulfates (NOS_i). Moreover, the variations in OS_i mass concentrations

297 ($\sim$2 times) were much larger than those in OS_i mass fractions (< 1.2 times). These

298 results indicate that the production of major OS_i (e.g., $C_5H_{11}O_7S^-$, $C_5H_9O_7S^-$ and

299 $C_5H_7O_7S^-$) was weakened during the nighttime. In contrast, the higher concentration

300 for these OS_i in the daytime can be attributed to the increased levels of precursors (e.g.,

301 isoprene) (Bryant et al. 2021) and oxidants (e.g., O_3) (**Table S5**) as well as the strong

302 photochemistry in the daytime. Although the average fraction of NOS_i was higher in

303 the nighttime than in the daytime, their concentration was similar between the daytime

304 and nighttime. This is because that several special NOS_i (e.g., $C_5H_{10}NO_9S^-$,

305 $C_5H_8NO_{10}S^-$, $C_4H_8NO_7S^-$, and $C_5H_8NO_7S^-$) peaked in the daytime, although

306 $C_5H_9N_2O_{11}S^-$ showed maximum in the nighttime (**Table S2**). Previous laboratory

307 studies have suggested that the formation of $C_5H_{10}NO_9S^-$ is mainly related to •OH

308 oxidation processes (Hamilton et al. 2021). Thus, a strong photochemical oxidation

309 during daytime can be responsible for the increases in concentrations of these NOS_i

310 (particularly $C_5H_{10}NO_9S^-$) from the nighttime to the daytime. Overall, the diurnal

311   variations of other OSs including OS_m, C_2-C_3 OSs, and OS_a were similar to that of OS_i,

312   with a higher level in the daytime than in the nighttime excepting for NOSs (**Figure 1**

313   and **Tables S2** and **S3**). It is noteworthy that the fractions and concentrations of

314   monoterpene-derived NOSs (NOS_m) were higher in the nighttime than in the daytime

315   (**Table S2**). This case can be attributed to NO_3•-related nighttime chemistry (Wang et

316   al. 2018). Thus, these findings further emphasize the importance of photochemistry for

317   daytime OS formation and nighttime chemistry for NOS (in particular NOS_m)

318   formation in urban Shanghai.

319   The concentrations of various types of OSs at the suburban site were lower than

320   those at the urban site in both daytime and nighttime (**Figures 1b,c**). However, the

321   characteristics of diurnal difference in various OSs at the suburban site were similar to

322   those observed at the urban site, which showed a substantially higher OS level in the

323   daytime. A similar case was also found in Beijing in 2016 (Wang et al. 2018) and

324   Shanghai in 2017 (Cai et al. 2020). Clearly, the aerosol OS abundance in Shanghai was

325   mainly controlled by the OS formation process in the daytime rather than in the

326   nighttime.

327

328   **3.2. Time series of the major OSs**

329   **Figures 2a-2h** compare the time series of the major OS species and inorganic ions

330   in $PM_{2.5}$ collected at urban and suburban sites. The OS_i concentrations peaked during

331   daytime on July 11 and 12, with maximum values of 479.8 ng m^{-3} and 309.5 ng m^{-3} at

332   urban and suburban sites, respectively. Owing to the high proportion of OS_i in total OSs,

total OS concentrations also showed maximum values during July 11 and 12. The mass

concentrations of total OSs, OS_i, and $C_5H_{11}O_7S^-$ (a major OS_i component) decreased

from July 11 to July 14 (period A; i.e., relatively polluted period) in both urban and

suburban areas, whereas their concentrations exhibited a quite small fluctuation after

July 14 (period B; i.e., clean period). As a result, the mean concentrations of total OSs

and OS_i were ~4 times higher in the period A than in the period B. The temporal

variations in the concentrations of OS_m, $C_8H_{13}O_7S^-$ (a major component of OS_m)

(Schindelka et al. 2013), OS_a, and C_2-C_3 OSs were similar to those of total OSs and OS_i.

However, the dissimilarities in the diurnal variations of OSs in period A and period B

suggest that the sources or levels of precursors and oxidants associated with OS

formation differed between these two periods. This consideration was further supported

by decreasing O_3 and NO_2 levels from period A to period B (**Table S5** and **Figures 2i,j**).

Sulfate showed a temporal variation similar to total OSs, OS_i, and OS_m

concentrations in most days (**Figures 2g,h**). We observed several abnormally high

sulfate events during period B (from the evening of the 17th to 18th). The transport

distance of air mass on July 18 was found to be shorter than that in other days (**Figure

S3**); moreover, VC value was lower on July 18 than on other days (**Figure S4**). Thus,

this high sulfate case can be partly attributed to the special meteorological conditions

on July 18. In general, sulfate concentrations showed a strong correlation with total OSs,

OS_i, and OS_m concentrations at both sites ($P < 0.01$, $r = 0.76$–0.78). These results

indicate that the abundances of OSs in these two study areas were tightly associated

with sulfate-related particle-phase chemistry (Surratt et al. 2008).

355   The concentrations of total OSs, OS_i, and OS_m exhibited a distinct diurnal

356 variation during period A at both sites, with a higher concentration in the daytime. The

357 diurnal variation pattern of OSs was similar to those of O_3 and sulfate. These findings

358 imply an important role of atmospheric oxidation capacity and sulfate in daytime OS

359 formation. Exceptionally, although a clear diurnal pattern was also observed for NOS_m,

360 their concentrations peaked in the nighttime, suggesting that the formation of NOS_m

361 was highly affected by the $NO_3\cdot$-related nighttime chemistry (Iinuma et al. 2007;

362 Surratt et al. 2008). In the period B, the concentrations of various OSs showed a weak

363 diurnal variation, with a slightly higher level in the daytime.

364   As mentioned above, the ambient levels of oxidants (e.g, O_3 and NO_2) and sulfates

365 showed a significant difference in period A and period B, which were tightly associated

366 with the formation of OSs (Wang et al. 2021). Cluster analysis of backward trajectories

367 showed that air masses arriving at both urban and suburban sites in the period A mainly

368 originated from the continental region, with significant influences of anthropogenic

369 emissions (e.g., NO_x and SO_2) from southern YRD. Furthermore, considering the

370 distinct and similar diurnal variation of O_3, NO_2, SO_2, sulfate, and OSs during period A

371 at both sites, aerosol OSs can be assumed to be mainly formed in local areas. In contrast,

372 these two sampling sites were primarily affected by air masses transported from the

373 East China Sea in the period B. Moreover, the average VC value in the period A was

374 two times lower than that in the period B (**Table S5**), implying relatively weaker

375 diffusion and dilution of air pollutants in the period A. These factors can be partly

376 responsible for the higher oxidant and sulfate concentrations in the period A than in the
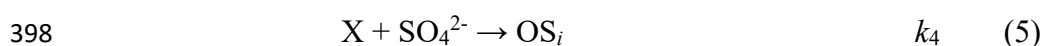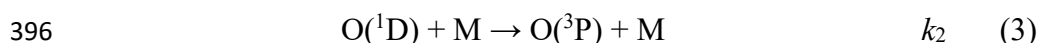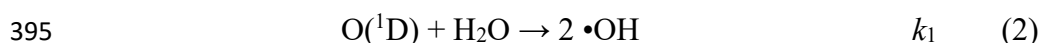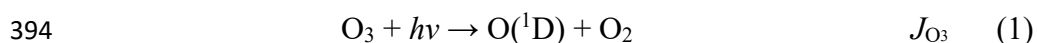
17

period B. Similarly, since the suburban site is closer to the East China Sea with a decreased influence from anthropogenic emissions (**Figure 3**), the levels of O_3, NO_x, and sulfate were higher at the urban site than at the suburban site (**Figure 2** and **Table S5**). The differences in the concentration of oxidants and sulfate might provide an explanation for the difference in the concentrations of OSs between periods A and B as well as between urban and suburban sites.

3.3. Formation mechanisms of OSs

3.3.1 Isoprene-derived OSs

Previous laboratory studies have suggested that isoprene can react with •OH to form IEPOX in the gas phase under low NO_x conditions (Fabien et al. 2009). In the daytime, ambient O_3 can be rapidly photolyzed to generate •OH under the influence of UV (Kourtchev et al. 2015). Thus, O_3 and UV could serve as a proxy of •OH. Considering a significant role of photochemistry and sulfate-related heterogeneous chemistry in the formation of OSs, OS_i production is expected to be closely associated with isoprene, O_3, UV, and sulfate. Specifically, the simplified pathways leading to the formation of OS_i in the atmosphere can be derived as follows.

$$O_3 + hv \rightarrow O(^1D) + O_2 \qquad\qquad J_{O_3} \quad (1)$$

$$O(^1D) + H_2O \rightarrow 2 \text{ •OH} \qquad\qquad k_1 \quad (2)$$

$$O(^1D) + M \rightarrow O(^3P) + M \qquad\qquad k_2 \quad (3)$$

$$\text{Isoprene} + \text{•OH} \rightarrow X \qquad\qquad k_3 \quad (4)$$

$$X + SO_4^{2-} \rightarrow OS_i \qquad\qquad k_4 \quad (5)$$

399   Where J_{O_3} is the photolysis rate constant, k_{1-4} is the second-order rate coefficient, M is

400   N_2 or O_2, and X represents the potential products (e.g., IEPOX and HMML) of isoprene

401   oxidation by •OH.

402   Assuming the concentrations of $O(^1D)$ and •OH are in the steady state, we can

403   derive the following equations (H. andSeinfeld 2016).

404    $$[O(^1D)] = \frac{J_{O_3}[O_3]}{k_1[H_2O] + k_2[M]} \qquad (6)$$

405    $$[\bullet OH] = 2\tau_{OH}k_1[O(^1D)][H_2O] \qquad (7)$$

406   Where τ_{OH} is the average lifetime of •OH. In general, J_{O_3} is linearly dependent on the

407   UV radiation, i.e., $J_{O_3} = \varphi UV$, where φ is the slope of the linear fitting between J_{O_3} and

408   UV radiation (Li et al. 2022). Combining equation (6) and (7), the steady-state •OH

409   concentration can be expressed as:

410    $$[\bullet OH] = \frac{2\tau_{OH}k_1[H_2O] J_{O_3}[O_3]}{k_1[H_2O] + k_2[M]} = \alpha\varphi\tau_{OH}UV[O_3] \qquad (8)$$

411    $$\alpha = \frac{2k_1[H_2O]}{k_1[H_2O] + k_2[M]} \qquad (9)$$

412   Also, assuming a steady-state to the oxygenated organic intermediates (i.e., X),

413   we can derive:

414    $$[X] = k_3\tau_X[Isoprene][OH] = \alpha\varphi k_3\tau_X\tau_{OH}[Isoprene]UV[O_3] \qquad (10)$$

415   Where τ_X is the average lifetime of X in the atmosphere.

416   During the strong formation of OS_i via the heterogeneous reactions of X on acidic

417   sulfate, the change in the abundance of OS_i is expected to be proportional to its

418   formation rate:

419    $$\frac{d[OS_i]}{dt} \propto k_4[SO_4^{2-}][X] \propto \alpha\varphi k_3 k_4\tau_X\tau_{OH}[Isoprene]UV[O_3][SO_4^{2-}] \qquad (11)$$

420   It should be noted that the above equations are derived based on the assumption

19

that the reaction between $O(^1D)$ and H_2O is a major source of summertime $\bullet OH$ in the studied areas. Given that a linear relationship was observed between atmospheric $\bullet OH$ and $J_{O(^1D)}$ in different atmospheres (Stone et al., 2012), such an assumption seems to be reasonable. When isoprene is in a steady state in the atmosphere, OS_i production is expected to be proportional to the product of O_3, UV, and sulfate.

$$\frac{d[OS_i]}{dt} \propto UV[O_3][SO_4^{2-}] \tag{12}$$

It should be noted that equation (12) did not consider the influences of aerosol acidity, ALW, and other factors (e.g., $\bullet OH$ production from the photolysis of nitrous acid and aldehydes during the daytime). However, the deduction can at least suggest that the secondary production of OS_i is positively correlated with the value of $UV[O_3][SO_4^{2-}]$. Indeed, the concentrations of daytime OS_i and major OS_i species showed a linear positive relationship with the value of $UV[O_3][SO_4^{2-}]$ at both urban and suburban sites ($r = 0.84$–0.92, $P < 0.01$) (**Figure 4a-c**). We found that the correlation between major OS_i species and $UV[O_3][SO_4^{2-}]$ was stronger than the correlation of major OS_i species with O_3 and SO_4^{2-} ($r < 0.82$, $P < 0.01$); moreover, there was no significant correlation between major OSs and UV ($P > 0.05$). Thus, our results provide field evidence that the formation of daytime OS_i in these two study areas was mainly controlled by $\bullet OH$ oxidation of isoprene; moreover, the higher concentration of OS_i in the urban area can be attributed to the stronger atmospheric oxidation capacity (i.e., higher $UV[O_3]$ value) and more serious anthropogenic sulfate pollution (particularly during period A). We also observed that the OS concentrations did not significantly increase in several high sulfate events in the period B. One possible explanation is that

443   these abnormal high sulfate events resulted in excessive SO_4^{2-} in the formation of OSs.

444   2-MT-OS and 2-MGA-OS have been identified as important tracers of isoprene-

445 derived SOA (Hettiyadura et al. 2019; Cai et al. 2020). During isoprene oxidation by

446 •OH, these two OS species are produced under low (i.e., IEPOX pathway) and high

447 (i.e., HMML or methacrylic acid epoxide (MAE) pathways) NO_x conditions,

448 respectively (Surratt et al. 2010; Nguyen et al. 2015). The ratios of 2-MT-OS

449 concentration to 2-MGA-OS concentration in the daytime were 9.7 ± 3.1 and $12.1 \pm$

450 5.5 at urban and suburban sites, respectively (**Figure S5b**). A 2-MT-OS/2-MGA-OS

451 ratio of larger than 1 was also found in observations in summer 2020 (**Figure S5a**),

452 suggesting low NO_x channel dominated the formation of daytime OS_i in the two study

453 areas. This finding was similar to previous observations in Beijing (3.2) (Wang et al.

454 2020) and Guangzhou (7.6) (Bryant et al. 2021). Other abundant OS_i compounds

455 including $C_5H_7O_7S^-$, $C_4H_7O_6S^-$, and $C_5H_9O_7S^-$ can be produced by the photooxidation

456 of isoprene, heterogeneous oxidative aging of 2-MT-OS, or sulfate radical-initiated

457 reaction with methacrolein and methyl vinyl ketone in the aqueous phase (Schindelka

458 et al. 2013; Wach et al. 2019; Hettiyadura et al. 2015). These OSs showed strong

459 correlations ($r = 0.74$–0.90, $P < 0.01$) with $UV[O_3][SO_4^{2-}]$, which further highlights the

460 significance of the photochemistry in OS_i formation.

461   In the nighttime, the formation •OH can be primarily attributed to the reactions of

462 olefins and O_3 (Paulson andOrlando 1996). As shown in **Figures 4d-f**, total OS_i and

463 major OS_i compounds were significantly correlated with the product of O_3 and SO_4^{2-}

464 concentrations ($P < 0.01$, $r = 0.96$–0.98). Since the nighttime oxidant level (including

465   O_3 and •OH) was substantially lower than that in the daytime (**Table S5**), the production

466   of OS_i was weakened in the nighttime (**Table S2**). It is interesting to note the 2-MT-

467   OS/2-MGA-OS mean ratio in the nighttime was 13.1–15.0 (**Figure S5(b)**), significantly

468   higher than the mean ratio (9.7–12.1) in the daytime, indicating that the IEPOX

469   pathway may be a potential mechanism to generate OS_i in the nighttime. Another

470   possible explanation for the decreased OS concentration in the nighttime is that these

471   OSs were mainly formed during the daytime, but had a lower abundance in the

472   nighttime due to deposition and weak nighttime formation. Namely, considering the

473   strong diffusion effect during the daytime and the weak diffusion effect at the nighttime

474   (**Figure S4**), the nighttime OSs may be partially derived from OSs formed via

475   photochemical processes during the daytime. This is because the enhanced diffusion

476   effect during the daytime can result in a decrease in the amount of OS produced during

477   the daytime to deposit into the nighttime.

478   Furthermore, NO_3• chemistry in the nighttime was another possible pathway to

479   form OS_i, particularly NOSs. The nighttime NOS concentration was linearly correlated

480   with the product of NO_2 and O_3 ($[NO_2][O_3]$, i.e., a proxy of NO_3•) (**Figure S6**).

481   Interestingly, most of NOS_i (e.g., $C_5H_{10}NO_9S^-$, $C_5H_8NO_{10}S^-$, $C_4H_8NO_7S^-$, and

482     $C_5H_8NO_7S^-$) have higher concentrations in the daytime, excepting for $C_5H_9N_2O_{11}S^-$.

483   Thus, although nighttime NO_3• chemistry was important, the NOS_i formed via

484   photochemistry under the influence of NO_x in the daytime was still dominant

485   contributors to total NOS_i in our study areas. Regarding $C_5H_9N_2O_{11}S^-$, its formation

486   pathway is mainly the NO_3• oxidation of $C_5H_9NO_5$ as illustrated in **Figure S7**

22

487 (Hamilton et al. 2021). Accordingly, the abundance of $C_5H_9N_2O_{11}S^-$ peaked during the

488 nighttime (**Figure S8**). It should be pointed out that the •OH oxidation of $C_5H_9NO_5$ can

489 also contribute to the production of $C_5H_{10}NO_9S^-$ (**Figure S7**). Clearly, this mechanism

490 can be responsible for the higher $C_5H_{10}NO_9S^-$ concentrations in the daytime as

491 mentioned above. In general, increased OS_i level in the daytime demonstrated that the

492 formation of OS_i in urban and suburban areas was largely controlled by photooxidation

493 of isoprene in the presence of sulfate in the daytime, rather than nighttime $NO_3•$

494 chemistry. Moreover, a decrease in average OS_i level from the urban area to the

495 suburban area can be explained by the weakened photooxidation of isoprene and the

496 decreased anthropogenic sulfate pollution (particularly in the relatively polluted period).

497

498 **3.3.2 Monoterpene-derived OSs**

499   The concentrations of the most abundant OS_m species ($C_{10}H_{15}O_7S^-$ and $C_8H_{13}O_7S^-$)

500 showed a strong correlation with the value of $UV[O_3][SO_4^{2-}]$ (and $UV[O_3][SO_2]$) in the

501 daytime at both urban and suburban sites ($r = 0.82–0.86$, $P < 0.01$), indicating that the

502 photooxidation of monoterpenes was a significant source for OS_m. Previous studies also

503 demonstrated that $C_{10}H_{15}O_7S^-$ can be produced through the photooxidation of

504 monoterpenes or sulfate radical reaction with α-pinene (Surratt et al. 2008; Nozière et

505 al. 2010).

506   In the nighttime, the concentrations of nitrogen-free OS_m species decreased

507 significantly with a decrease in the O_3 levels (Wang et al. 2020). However, NOS_m

508 species increased in concentration in the nighttime and showed a significant correlation

509   with the value of $[O_3][NO_2]$ (the proxy of $NO_3\bullet$, as mentioned above) ($r = 0.90\text{–}0.95$, P

510   < 0.01). Accordingly, nighttime $NO_3\bullet$ chemistry exerted a significant influence on the

511   abundance of NOS_m in these study areas. A study by Hamilton et al., (Hamilton et al.

512   2021) has reported that $NO_3\bullet$ chemistry plays an important role in the production of

513   NOS_m. However, the overall lower OS_m level in the nighttime (**Table S2**) suggests that

514   daytime OS_m production via monoterpenes photooxidation was still the dominant

515   contributor to total OS_m throughout the day. Although several filed studies have

516   reported the abundance of various NOS_m (e.g., $C_{10}H_{16}NO_7S^-$ and $C_9H_{14}NO_8S^-$) (Wang

517   et al. 2018; Bryant et al. 2021; Cai et al. 2020), their structures, formation mechanisms,

518   and relevant diurnal variations remain large uncertainties, which need to be deeply

519   explored in the future research.

520

521   **3.3.3 C₂-C₃ and anthropogenic OSs**

522   The OS species with two or three carbon atoms ($C_2\text{-}C_3$ OSs) are generally

523   considered to originate from both biogenic and anthropogenic emissions (Wang et al.

524   2020). The abundant $C_2\text{-}C_3$ OS species, including $C_2H_3O_6S^-$ (glycolic acid sulfate;

525   GAS), $C_3H_5O_5S^-$ (hydroxyacetone sulfate; HAS), and $C_3H_5O_6S^-$ (lactic acid sulfate;

526   LAS), were significantly correlated with the values of $UV[O_3][SO_4^{2-}]$ in the daytime at

527   both urban and suburban sites ($r = 0.79\text{–}0.91$, $P < 0.01$), indicating that the

528   photochemical processes largely contributed to the formation of $C_2\text{-}C_3$ OSs. Recently,

529   the heterogeneous $\bullet$OH oxidation of particulate 2-MT-OS has been shown to generate

530   a series of $C_2\text{-}C_3$ OSs (e.g., $C_2H_3O_6S^-$, $C_3H_5O_6S^-$, and $C_2H_3O_5S^-$) (Chen et al. 2020).

531   Moreover, $C_3H_5O_4S^-$ and $C_3H_7O_5S^-$ have previously been reported to be produced by

532   the photooxidation of diesel vehicle exhausts (Blair et al. 2017).

533   Most of the quantified OS_a compounds, including $C_{13}H_{25}O_5S^-$, $C_9H_{15}O_7S^-$,

534     $C_8H_{17}O_4S^-$, benzyl sulfate ($C_7H_7O_4S^-$), phenyl sulfate ($C_6H_5O_4S^-$), as well as

535     $C_6H_9O_6S^-$, $C_5H_7O_6S^-$, and $C_4H_7O_4S^-$, exhibited a strong correlation ($P < 0.01$) with the

536   values of $UV[O_3][SO_4^{2-}]$ in the daytime. $C_{13}H_{25}O_5S^-$ has been detected in diesel exhaust

537   (Cui et al. 2019), which is the homologous compound of $C_{12}H_{23}O_5S^-$ produced from

538   dodecane photooxidation (Riva et al. 2016b). A chamber study has detected $C_9H_{15}O_7S^-$

539   in decalin SOA and speculated that it was produced via •OH oxidation of a C_9-carbonyl

540   hydroperoxide ($C_9H_{16}O_3$) and subsequent reaction on acidic sulfate aerosols (Riva et al.

541   2016b). In addition, photooxidation of diesel fuel vapor in the presence of SO_2 has been

542   suggested to be an important source of $C_6H_9O_6S^-$, $C_5H_7O_6S^-$, and $C_4H_7O_4S^-$ species

543   (Blair et al. 2017). The formation of $C_7H_7O_4S^-$ and $C_6H_5O_4S^-$ can also be attributed to

544   the photooxidation of naphthalene and 2-methylnaphthalene (Riva et al. 2015).

545   We note that the concentrations of most of C_2-C_3 OS and OS_a species decreased

546   significantly from the daytime to the nighttime (**Table S2** and **Table S3**). As discussed

547   above, the OSs observed in the nighttime may partially come from the OSs generated

548   during the daytime. Thus, the deposition effect from the daytime to the nighttime was

549   an important factor controlling nighttime levels of C_2-C_3 OSs and OS_a. In addition, the

550   nighttime gas-phase oxidation process was also likely associated with C_2-C_3 and

551   anthropogenic OS formation at both urban and suburban sites, as suggested by the

552   significant correlations of C_2-C_3 OSs and OS_a with O_3 and $[O_3][NO_2]$ in the nighttime

553 (r = 0.89–0.91, P < 0.01). Overall, these results further highlight the importance of

554 photochemistry in controlling the all-day abundance of OSs, as discussed earlier.

555

3.3.4 The effects of ALW and pH on OS formation

557 　　We have demonstrated that the atmospheric oxidation capacity (e.g., UV[O_3] and

558 [O_3 + NO_2]), sulfate pollution, and nighttime NO_3• chemistry exerted considerable

559 influences on the formation of OSs in both urban and suburban areas. In addition,

560 laboratory and field studies have suggested that aerosol properties including acidity and

561 ALW also play important roles in OS formation (Iinuma et al. 2007; Surratt et al. 2007b;

562 Wang et al. 2020; Wang et al. 2018; 2022). The aerosol pH in Shanghai in summer

563 averaged 2.7 ± 0.9 and 2.2 ± 0.7 in urban and suburban areas, respectively. The mean

564 pH value was similar to that in northern China (summer) (Ding et al. 2019; Wang et al.

565 2018), but higher than that in the Pearl River Delta (PRD) region (Fu et al. 2015). In

566 this study, only the 2-MT-OS concentration showed an evident negative correlation with

567 the pH value (r = 0.58, P < 0.05), suggesting the aerosol acidity is not a limiting factor

568 for the formation of most OS species.

569 　　A positive correlation was observed between the concentrations of OSs and ALW

570 only in the urban area during both daytime and nighttime (**Figure 5**), consistent with

571 our previous observations in urban Shanghai (Wang et al. 2021). It is interesting to note

572 that although higher ALW concentrations and lower pH values were observed at the

573 suburban site, the OS concentrations were significantly higher at the urban site (**Table**

574 **S5**). This result further confirms that atmospheric oxidation capacity and sulfate

575 pollution level governed the formation of OSs in urban and suburban Shanghai

576 (particularly in the relatively polluted period), though ALW and aerosol acidity also

577 played a role. Therefore, a synergistic regulation of atmospheric oxidation capacity and

578 anthropogenic SO_2 emissions would be important for the mitigation of OS and SOA

579 pollution in the megacity Shanghai.

580

581 **4. Conclusions**

582 We investigated the spatial and diurnal variations of aerosol OS formation in

583 Shanghai in summer. Isoprene- and monoterpene-derived OSs were found to be the

584 dominant OS groups during the entire sampling campaign, likely suggesting that the

585 formation of OSs was largely controlled by biogenic VOCs. Most OSs decreased from

586 the daytime to the nighttime, while NOS_m peaked during nighttime. These findings

587 suggested that OSs were mainly produced via daytime formation processes in both

588 urban and suburban areas, except for NOS_m. Moreover, the average abundance of

589 various types of OSs showed a decrease trend from the urban area to the suburban area,

590 which can be explained by weakened atmospheric oxidation capacity and sulfate

591 pollution in the suburban area (primarily in the relatively polluted period). Further,

592 daytime OS formation was concretized according to the interactions among OSs, UV,

593 O_3, and SO_4^{2-}, suggesting that the concentrations of most OSs were significantly

594 correlated with the values of $UV[O_3][SO_4^{2-}]$ during daytime in both urban and suburban

595 Shanghai. We concluded that an enhancement in the photochemical process and sulfate

596 level can exacerbate OS pollution in the urban area. These findings were summarized

in a diagram (**Figure 6**). Generally, our study not only deepens the understanding about the importance of photochemical process and anthropogenic sulfate pollution in controlling OS formation but also provides potential management strategies to decrease the abundance of particulate OSs.

Data availability

The data presented in this work are available upon request from the corresponding authors.

Supplement

The supplement related to this article is available online.

Competing interests

The authors declare no competing financial interest.

Author contributions. TY, QY, and Y-J.M performed field measurements; TY performed chemical analysis; YX, TY, and YZ performed data analysis; YX and TY wrote the original manuscript; and YX, YZ, Y-C.W, J-Z.Y, Y-S.D, C-X.L, H-W.X, Z-Y.L, and H-Y.X reviewed and edited the manuscript.

References

Berndt, T., Richters, S., Jokinen, T., Hyttinen, N., Kurten, T., Otkjaer, R. V., Kjaergaard, H. G., Stratmann, F., Herrmann, H., Sipila, M., Kulmala, M., and Ehn, M.: Hydroxyl radical-induced formation of highly oxidized organic compounds, Nat. Commun., 7, 13677, 10.1038/ncomms13677, 2016.

Blair, S. L., MacMillan, A. C., Drozd, G. T., Goldstein, A. H., Chu, R. K., Pasa-Tolic, L., Shaw, J. B., Tolic, N., Lin, P., Laskin, J., Laskin, A., and Nizkorodov, S. A.: Molecular Characterization of Organosulfur Compounds in Biodiesel and Diesel Fuel Secondary Organic Aerosol, Environ. Sci. Technol., 51, 119-127, 10.1021/acs.est.6b03304, 2017.

Brüggemann, M., Riva, M., Perrier, S., Poulain, L., George, C., and Herrmann, H.: Overestimation of Monoterpene Organosulfate Abundance in Aerosol Particles by Sampling in the Presence of SO2, Environmental Science & Technology Letters, 8, 206-211, 10.1021/acs.estlett.0c00814, 2021.

641   Bryant, D. J., Elzein, A., Newland, M., White, E., Swift, S., Watkins, A., Deng, W.,

642   Song, W., Wang, S., Zhang, Y., Wang, X., Rickard, A. R., and Hamilton, J. F.:

643   Importance of Oxidants and Temperature in the Formation of Biogenic

644   Organosulfates and Nitrooxy Organosulfates, ACS Earth Space Chem., 5, 2291-

645   2306, 10.1021/acsearthspacechem.1c00204, 2021.

646   Budisulistiorini, S. H., Li, X., Bairai, S. T., Renfro, J., Liu, Y., Liu, Y. J., McKinney, K.

647   A., Martin, S. T., McNeill, V. F., Pye, H. O. T., Nenes, A., Neff, M. E., Stone, E.

648   A., Mueller, S., Knote, C., Shaw, S. L., Zhang, Z., Gold, A., and Surratt, J. D.:

649   Examining the effects of anthropogenic emissions on isoprene-derived

650   secondary organic aerosol formation during the 2013 Southern Oxidant and

651   Aerosol Study (SOAS) at the Look Rock, Tennessee ground site, Atmospheric

652   Chemistry and Physics, 15, 8871-8888, 10.5194/acp-15-8871-2015, 2015.

653   Cai, D., Wang, X., Chen, J., and Li, X.: Molecular Characterization of Organosulfates

654   in Highly Polluted Atmosphere Using Ultra-High-Resolution Mass

655   Spectrometry, J. Geophys. Res.: Atmos. , 125, 10.1029/2019jd032253, 2020.

656   Chen, Y., Dombek, T., Hand, J., Zhang, Z., Gold, A., Ault, A. P., Levine, K. E., and

657   Surratt, J. D.: Seasonal Contribution of Isoprene-Derived Organosulfates to

658   Total Water-Soluble Fine Particulate Organic Sulfur in the United States, ACS

659   Earth and Space Chemistry, 5, 2419-2432,

660   10.1021/acsearthspacechem.1c00102, 2021.

661   Chen, Y., Zhang, Y., Lambe, A. T., Xu, R., Lei, Z., Olson, N. E., Zhang, Z., Szalkowski,

662   T., Cui, T., Vizuete, W., Gold, A., Turpin, B. J., Ault, A. P., Chan, M. N., and

Surratt, J. D.: Heterogeneous Hydroxyl Radical Oxidation of Isoprene-Epoxydiol-Derived Methyltetrol Sulfates: Plausible Formation Mechanisms of Previously Unexplained Organosulfates in Ambient Fine Aerosols, Environ. Sci. Technol.Lett., 7, 460-468, 10.1021/acs.estlett.0c00276, 2020.

Cui, M., Li, C., Chen, Y., Zhang, F., Li, J., Jiang, B., Mo, Y., Li, J., Yan, C., Zheng, M., Xie, Z., Zhang, G., and Zheng, J.: Molecular characterization of polar organic aerosol constituents in off-road engine emissions using Fourier transform ion cyclotron resonance mass spectrometry (FT-ICR MS): implications for source apportionment, Atmos. Chem. Phys., 19, 13945-13956, 10.5194/acp-19-13945-2019, 2019.

Cui, T., Zeng, Z., dos Santos, E. O., Zhang, Z., Chen, Y., Zhang, Y., Rose, C. A., Budisulistiorini, S. H., Collins, L. B., Bodnar, W. M., de Souza, R. A. F., Martin, S. T., Machado, C. M. D., Turpin, B. J., Gold, A., Ault, A. P., and Surratt, J. D.: Development of a hydrophilic interaction liquid chromatography (HILIC) method for the chemical characterization of water-soluble isoprene epoxydiol (IEPOX)-derived secondary organic aerosol, Environmental Science: Processes & Impacts, 20, 1524-1536, 10.1039/c8em00308d, 2018.

Ding, J., Zhao, P., Su, J., Dong, Q., Du, X., and Zhang, Y.: Aerosol pH and its driving factors in Beijing, Atmos. Chem. Phys., 19, 7939-7954, 10.5194/acp-19-7939-2019, 2019.

Ding, S., Chen, Y., Devineni, S. R., Pavuluri, C. M., and Li, X. D.: Distribution characteristics of organosulfates (OSs) in PM2.5 in Tianjin, Northern China:

Quantitative analysis of total and three OS species, Sci. Total. Environ., 834, 155314, 10.1016/j.scitotenv.2022.155314, 2022.

Estillore, A. D., Hettiyadura, A. P., Qin, Z., Leckrone, E., Wombacher, B., Humphry, T., Stone, E. A., and Grassian, V. H.: Water Uptake and Hygroscopic Growth of Organosulfate Aerosol, Environ Sci Technol, 50, 4259-4268, 10.1021/acs.est.5b05014, 2016.

Fabien, P., John, D. C., Henrik, G. K., Andreas, k., Jason, M. S. C., John, H. S., and Paul, O. W.: Unexpected Epoxide Formation in the Gas-Phase Photooxidation of Isoprene, Science, 325, 730-733, 2009.

Fleming, L. T., Ali, N. N., Blair, S. L., Roveretto, M., George, C., and Nizkorodov, S. A.: Formation of Light-Absorbing Organosulfates during Evaporation of Secondary Organic Material Extracts in the Presence of Sulfuric Acid, ACS Earth Space Chem., 3, 947-957, 10.1021/acsearthspacechem.9b00036, 2019.

Fu, X., Guo, H., Wang, X., Ding, X., He, Q., Liu, T., and Zhang, Z.: PM2.5 acidity at a background site in the Pearl River Delta region in fall-winter of 2007-2012, J. Hazard. Mater., 286, 484-492, 10.1016/j.jhazmat.2015.01.022, 2015.

Gani, S., Bhandari, S., Seraj, S., Wang, D. S., Patel, K., Soni, P., Arub, Z., Habib, G., Hildebrandt Ruiz, L., and Apte, J. S.: Submicron aerosol composition in the world's most polluted megacity: the Delhi Aerosol Supersite study, Atmos. Chem. Phys., 19, 6843-6859, 10.5194/acp-19-6843-2019, 2019.

Glasius, M., Thomsen, D., Wang, K., Iversen, L. S., Duan, J., and Huang, R. J.: Chemical characteristics and sources of organosulfates, organosulfonates, and

carboxylic acids in aerosols in urban Xi'an, Northwest China, Sci Total Environ, 810, 151187, 10.1016/j.scitotenv.2021.151187, 2022.

Guo, H., Xu, L., Bougiatioti, A., Cerully, K. M., Capps, S. L., Hite Jr, J. R., Carlton, A. G., Lee, S. H., Bergin, M. H., Ng, N. L., Nenes, A., and Weber, R. J.: Fine-particle water and pH in the southeastern United States, Atmos. Chem. Phys., 15, 5211-5228, 10.5194/acp-15-5211-2015, 2015.

Guo, Q., Wei, Y., and Wan, R.: Leading officials' accountability audit of natural resources and haze pollution: evidence from China, Environmental Science and Pollution Research, 30, 17612-17628, 10.1007/s11356-022-23340-x, 2022.

H., J. and Seinfeld, S. N. P.: Atmospheric chemistry and physics: from air pollution to climate change, 2016.

Hamilton, J. F., Bryant, D. J., Edwards, P. M., Ouyang, B., Bannan, T. J., Mehra, A., Mayhew, A. W., Hopkins, J. R., Dunmore, R. E., Squires, F. A., Lee, J. D., Newland, M. J., Worrall, S. D., Bacak, A., Coe, H., Percival, C., Whalley, L. K., Heard, D. E., Slater, E. J., Jones, R. L., Cui, T., Surratt, J. D., Reeves, C. E., Mills, G. P., Grimmond, S., Sun, Y., Xu, W., Shi, Z., and Rickard, A. R.: Key Role of NO3 Radicals in the Production of Isoprene Nitrates and Nitrooxyorganosulfates in Beijing, Environ. Sci. Technol., 55, 842-853, 10.1021/acs.est.0c05689, 2021.

Hansen, A. M. K., Kristensen, K., Nguyen, Q. T., Zare, A., Cozzi, F., Nøjgaard, J. K., Skov, H., Brandt, J., Christensen, J. H., Ström, J., Tunved, P., Krejci, R., and Glasius, M.: Organosulfates and organic acids in Arctic aerosols: speciation,

annual variation and concentration levels, Atmos. Chem. Phys., 14, 7807-7823, 10.5194/acp-14-7807-2014, 2014.

Hawkins, L. N., Russell, L. M., Covert, D. S., Quinn, P. K., and Bates, T. S.: Carboxylic acids, sulfates, and organosulfates in processed continental organic aerosol over the southeast Pacific Ocean during VOCALS-REx 2008, J. Geophys. Res.: Atmos. , 115, 10.1029/2009jd013276, 2010.

Hennigan, C. J., Izumi, J., Sullivan, A. P., Weber, R. J., and Nenes, A.: A critical evaluation of proxy methods used to estimate the acidity of atmospheric particles, Atmos. Chem. Phys., 15, 2775-2790, 10.5194/acp-15-2775-2015, 2015.

Hettiyadura, A. P. S., Al-Naiema, I. M., Hughes, D. D., Fang, T., and Stone, E. A.: Organosulfates in Atlanta, Georgia: anthropogenic influences on biogenic secondary organic aerosol formation, Atmos. Chem. Phys., 19, 3191-3206, 10.5194/acp-19-3191-2019, 2019.

Hettiyadura, A. P. S., Stone, E. A., Kundu, S., Baker, Z., Geddes, E., Richards, K., and Humphry, T.: Determination of atmospheric organosulfates using HILIC chromatography with MS detection, Atoms. Meas. Tech., 8, 2347-2358, 10.5194/amt-8-2347-2015, 2015.

Hettiyadura, A. P. S., Jayarathne, T., Baumann, K., Goldstein, A. H., de Gouw, J. A., Koss, A., Keutsch, F. N., Skog, K., and Stone, E. A.: Qualitative and quantitative analysis of atmospheric organosulfates in Centreville, Alabama, Atmos. Chem. Phys., 17, 1343-1359, 10.5194/acp-17-1343-2017, 2017.

751 Hettiyadura, A. P. S., Xu, L., Jayarathne, T., Skog, K., Guo, H., Weber, R. J., Nenes, A.,

752   Keutsch, F. N., Ng, N. L., and Stone, E. A.: Source apportionment of organic

753   carbon in Centreville, AL using organosulfates in organic tracer-based positive

754   matrix   factorization,   Atmospheric   Environment,   186,   74-88,

755   10.1016/j.atmosenv.2018.05.007, 2018.

756 Hughes, D. D., Christiansen, M. B., Milani, A., Vermeuel, M. P., Novak, G. A., Alwe,

757   H. D., Dickens, A. F., Pierce, R. B., Millet, D. B., Bertram, T. H., Stanier, C. O.,

758   and Stone, E. A.: PM2.5 chemistry, organosulfates, and secondary organic

759   aerosol during the 2017 Lake Michigan Ozone Study, Atmos. Environ., 244,

760   10.1016/j.atmosenv.2020.117939, 2021.

761 Iinuma , Müller , Berndt , Böge , Claeys，, and Herrmann: Evidence for the

762   Existence of Organosulfates from β-Pinene Ozonolysis in Ambient Secondary

763   Organic Aerosol, Environ. Sci. Technol., 41, 6678-6683, 2007.

764 Iinuma, Y., Müller, C., Böge, O., Gnauk, T., and Herrmann, H.: The formation of

765   organic sulfate esters in the limonene ozonolysis secondary organic aerosol

766   (SOA)   under   acidic   conditions,   Atmos.   Environ.,   41,   5571-5583,

767   10.1016/j.atmosenv.2007.03.007, 2007.

768 Jiang, H., Li, J., Tang, J., Cui, M., Zhao, S., Mo, Y., Tian, C., Zhang, X., Jiang, B., Liao,

769   Y., Chen, Y., and Zhang, G.: Molecular characteristics, sources, and formation

770   pathways of organosulfur compounds in ambient aerosol in Guangzhou, South

771   China, Atmos. Chem. Phys., 22, 6919-6935, 10.5194/acp-22-6919-2022, 2022.

772 Kanellopoulos, P. G., Kotsaki, S. P., Chrysochou, E., Koukoulakis, K., Zacharopoulos,

N., Philippopoulos, A., and Bakeas, E.: PM2.5-bound organosulfates in two Eastern Mediterranean cities: The dominance of isoprene organosulfates, Chemosphere, 297, 134103, 10.1016/j.chemosphere.2022.134103, 2022.

Kourtchev, I., Doussin, J. F., Giorio, C., Mahon, B., Wilson, E. M., Maurin, N., Pangui, E., Venables, D. S., Wenger, J. C., and Kalberer, M.: Molecular composition of fresh and aged secondary organic aerosol from a mixture of biogenic volatile compounds: a high-resolution mass spectrometry study, Atmos. Chem. Phys., 15, 5683-5695, 10.5194/acp-15-5683-2015, 2015.

Kristensen, K., Bilde, M., Aalto, P. P., Petäjä, T., and Glasius, M.: Denuder/filter sampling of organic acids and organosulfates at urban and boreal forest sites: Gas/particle distribution and possible sampling artifacts, Atmospheric Environment, 130, 36-53, 10.1016/j.atmosenv.2015.10.046, 2016.

Li, X., Zhang, Y., Shi, L., Kawamura, K., Kunwar, B., Takami, A., Arakaki, T., and Lai, S.: Aerosol Proteinaceous Matter in Coastal Okinawa, Japan: Influence of Long-Range Transport and Photochemical Degradation, Environ Sci Technol, 56, 5256-5265, 10.1021/acs.est.1c08658, 2022.

Lin, Y. H., Knipping, E. M., Edgerton, E. S., Shaw, S. L., and Surratt, J. D.: Investigating the influences of SO_2 and NH_3 levels on isoprene-derived secondary organic aerosol formation using conditional sampling approaches, Atmospheric Chemistry and Physics, 13, 8457-8470, 10.5194/acp-13-8457-2013, 2013.

Menon, S., ;, Unger, N., ;, Koch, D., ;, Francis, J., ;, Garrett, T., ;, Sednev, I., ;, Shindell,

D., ;, and Streets, D., ;: Aerosol climate effects and air quality impacts from
1980 to 2030, Environ. Res. Lett., 3, 10.1088/1748-9326/3/2/024004, 2008.

Nestorowicz, K., Jaoui, M., Rudzinski, K. J., Lewandowski, M., Kleindienst, T. E.,
Spolnik, G., Danikiewicz, W., and Szmigielski, R.: Chemical composition of
isoprene SOA under acidic and non-acidic conditions: effect of relative
humidity, Atmos Chem Phys, 18, 18101-18121, 10.5194/acp-18-18101-2018,
2018.

Nguyen, Q. T., Christensen, M. K., Cozzi, F., Zare, A., Hansen, A. M. K., Kristensen,
K., Tulinius, T. E., Madsen, H. H., Christensen, J. H., Brandt, J., Massling, A.,
Nøjgaard, J. K., and Glasius, M.: Understanding the anthropogenic influence on
formation of biogenic secondary organic aerosols in Denmark via analysis of
organosulfates and related oxidation products, Atmos. Chem. Phys., 14, 8961-
8981, 10.5194/acp-14-8961-2014, 2014.

Nguyen, T. B., Bates, K. H., Crounse, J. D., Schwantes, R. H., Zhang, X., Kjaergaard,
H. G., Surratt, J. D., Lin, P., Laskin, A., Seinfeld, J. H., and Wennberg, P. O.:
Mechanism of the hydroxyl radical oxidation of methacryloyl peroxynitrate
(MPAN) and its pathway toward secondary organic aerosol formation in the
atmosphere, Phys. Chem. Chem. Phys., 17, 17914-17926, 10.1039/c5cp02001h,
2015.

Nozière, B., Ekström, S., Alsberg, T., and Holmström, S.: Radical-initiated formation
of organosulfates and surfactants in atmospheric aerosols, Geophys. Res. Lett.,
37, n/a-n/a, 10.1029/2009gl041683, 2010.

817   O'Brien, R. E., Laskin, A., Laskin, J., Rubitschun, C. L., Surratt, J. D., and Goldstein,

818   A. H.: Molecular characterization of S- and N-containing organic constituents

819   in ambient aerosols by negative ion mode high-resolution Nanospray

820   Desorption Electrospray Ionization Mass Spectrometry: CalNex 2010 field

821   study, Journal of Geophysical Research: Atmospheres, 119,

822   10.1002/2014jd021955, 2014.

823   Olson, C. N., Galloway, M. M., Yu, G., Hedman, C. J., Lockett, M. R., Yoon, T., Stone,

824   E. A., Smith, L. M., and Keutsch, F. N.: Hydroxycarboxylic acid-derived

825   organosulfates: synthesis, stability, and quantification in ambient aerosol,

826   Environ Sci Technol, 45, 6468-6474, 10.1021/es201039p, 2011.

827   Passananti, M., Kong, L., Shang, J., Dupart, Y., Perrier, S., Chen, J., Donaldson, D. J.,

828   and George, C.: Organosulfate Formation through the Heterogeneous Reaction

829   of Sulfur Dioxide with Unsaturated Fatty Acids and Long-Chain Alkenes,

830   Angew. Chem. Int. Ed. Engl., 55, 10336-10339, 10.1002/anie.201605266, 2016.

831   Paulson, S. E. and Orlando, J. J.: The reactions of ozone with alkenes: An important

832   source of HOxin the boundary layer, Geophys. Res. Lett., 23, 3727-3730,

833   10.1029/96gl03477, 1996.

834   Pei, Z., Chen, X., Li, X., Liang, J., Lin, A., Li, S., Yang, S., Bin, J., and Dai, S.: Impact

835   of macroeconomic factors on ozone precursor emissions in China, Journal of

836   Cleaner Production, 344, 10.1016/j.jclepro.2022.130974, 2022.

837   Ramanathan , V., Crutzen, P. J., Kiehl, J. T., and Rosenfeld, D.: Aerosols, Climate, and

838   the Hydrological Cycle, Science, 294, 2119-2124, 2001.

839   Rattanavaraha, W., Chu, K., Budisulistiorini, S. H., Riva, M., Lin, Y. H., Edgerton, E.

840   S., Baumann, K., Shaw, S. L., Guo, H., King, L., Weber, R. J., Neff, M. E., Stone,

841   E. A., Offenberg, J. H., Zhang, Z., Gold, A., and Surratt, J. D.: Assessing the

842   impact of anthropogenic pollution on isoprene-derived secondary organic

843   aerosol formation in PM2.5 collected from the Birmingham, Alabama, ground

844   site during the 2013 Southern Oxidant and Aerosol Study, Atmos. Chem. Phys.,

845   16, 4897-4914, 10.5194/acp-16-4897-2016, 2016.

846   Riva, M., Budisulistiorini, S. H., Zhang, Z., Gold, A., and Surratt, J. D.: Chemical

847   characterization of secondary organic aerosol constituents from isoprene

848   ozonolysis in the presence of acidic aerosol, Atmospheric Environment, 130, 5-

849   13, 10.1016/j.atmosenv.2015.06.027, 2016a.

850   Riva, M., Da Silva Barbosa, T., Lin, Y.-H., Stone, E. A., Gold, A., and Surratt, J. D.:

851   Chemical characterization of organosulfates in secondary organic aerosol

852   derived from the photooxidation of alkanes, Atmos. Chem. Phys., 16, 11001-

853   11018, 10.5194/acp-16-11001-2016, 2016b.

854   Riva, M., Tomaz, S., Cui, T., Lin, Y. H., Perraudin, E., Gold, A., Stone, E. A., Villenave,

855   E., and Surratt, J. D.: Evidence for an unrecognized secondary anthropogenic

856   source of organosulfates and sulfonates: gas-phase oxidation of polycyclic

857   aromatic hydrocarbons in the presence of sulfate aerosol, Environ. Sci. Technol.,

858   49, 6654-6664, 10.1021/acs.est.5b00836, 2015.

859   Riva, M., Chen, Y., Zhang, Y., Lei, Z., Olson, N. E., Boyer, H. C., Narayan, S., Yee, L.

860   D., Green, H. S., Cui, T., Zhang, Z., Baumann, K., Fort, M., Edgerton, E.,

861   Budisulistiorini, S. H., Rose, C. A., Ribeiro, I. O., RL, E. O., Dos Santos, E. O.,

862   Machado, C. M. D., Szopa, S., Zhao, Y., Alves, E. G., de Sa, S. S., Hu, W.,

863   Knipping, E. M., Shaw, S. L., Duvoisin Junior, S., de Souza, R. A. F., Palm, B.

864   B., Jimenez, J. L., Glasius, M., Goldstein, A. H., Pye, H. O. T., Gold, A., Turpin,

865   B. J., Vizuete, W., Martin, S. T., Thornton, J. A., Dutcher, C. S., Ault, A. P., and

866   Surratt, J. D.: Increasing Isoprene Epoxydiol-to-Inorganic Sulfate Aerosol Ratio

867   Results in Extensive Conversion of Inorganic Sulfate to Organosulfur Forms:

868   Implications for Aerosol Physicochemical Properties, Environ. Sci. Technol., 53,

869   8682-8694, 10.1021/acs.est.9b01019, 2019.

870 Schindelka, J., Iinuma, Y., Hoffmann, D., and Herrmann, H.: Sulfate radical-initiated

871   formation of isoprene-derived organosulfates in atmospheric aerosols, Faraday

872   Discuss., 165, 237-259, 10.1039/c3fd00042g, 2013.

873 Shalamzari, M. S., Ryabtsova, O., Kahnt, A., Vermeylen, R., Herent, M. F., Quetin-

874   Leclercq, J., Van der Veken, P., Maenhaut, W., and Claeys, M: Mass

875   spectrometric characterization of organosulfates related to secondary organic

876   aerosol from isoprene, Rapid Commun. Mass Spectrom., 784-794,

877   10.1002/rcm.6511, 2013, 2013.

878 Shang, J., Passananti, M., Dupart, Y., Ciuraru, R., Tinel, L., Rossignol, S., Perrier, S.,

879   Zhu, T., and George, C.: SO2 Uptake on Oleic Acid: A New Formation Pathway

880   of Organosulfur Compounds in the Atmosphere, Environ. Sci. Technol.Lett., 3,

881   67-72, 10.1021/acs.estlett.6b00006, 2016.

882 Staudt, S., Kundu, S., Lehmler, H. J., He, X., Cui, T., Lin, Y. H., Kristensen, K., Glasius,

M., Zhang, X., Weber, R. J., Surratt, J. D., and Stone, E. A.: Aromatic organosulfates in atmospheric aerosols: synthesis, characterization, and abundance, Atmos Environ (1994), 94, 366-373, 10.1016/j.atmosenv.2014.05.049, 2014.

Stone, E. A., Yang, L., Yu, L. E., and Rupakheti, M.: Characterization of organosulfates in atmospheric aerosols at Four Asian locations, Atmos. Environ., 47, 323-329, 10.1016/j.atmosenv.2011.10.058, 2012.

Surratt, J. D., Lewandowski, M., Offenberg, J. H., Jaoui, M., Kleindienst, T.E., Edney, E. O., and Seinfeld, J. H.: Effect of Acidity on Secondary Organic Aerosol Formation from Isoprene, Environ. Sci. Technol., 41, 5363–5369, 2007a.

Surratt, J. D., Chan, A. W., Eddingsaas, N. C., Chan, M., Loza, C. L., Kwan, A. J., Hersey, S. P., Flagan, R. C., Wennberg, P. O., and Seinfeld, J. H.: Reactive intermediates revealed in secondary organic aerosol formation from isoprene, Proc. Natl. Acad. Sci. U.S.A., 107, 6640-6645, 10.1073/pnas.0911114107, 2010.

Surratt, J. D., Kroll, J. H., Kleindienst, T. E., Edney, E. O., Claeys, M., Sorooshian, A., Ng, N. L., Offenberg, J. H., Lewandowski, M., Jaoui, M., Flagan, R. C., and Seinfeld, J. H.: Evidence for Organosulfates in Secondary Organic Aerosol, Environ. Sci. Technol., 41, 517–527, 2007b.

Surratt, J. D., Gómez-González, Y., Chan, A. W. H., Vermeylen, R., Shahgholi, M., Kleindienst, T. E., Edney, E. O., Offenberg, J. H., Lewandowski, M., Jaoui, M., Maenhaut, W., Claeys, M., Flagan, R. C., and Seinfeld, J. H.: Organosulfate Formation in Biogenic Secondary Organic Aerosol, J. Phys. Chem. A., 112,

905   8345-8378, 10.1021/jp802310p, 2008.

906   Tolocka, M. P. and Turpin, B.: Contribution of organosulfur compounds to organic

907   aerosol mass, Environ. Sci. Technol., 46, 7978-7983, 10.1021/es300651v, 2012.

908   Turpin, B. J. and Lim, H.-J.: Species Contributions to PM2.5 Mass Concentrations:

909   Revisiting Common Assumptions for Estimating Organic Mass, Aerosol

910   Sci.Technol., 35, 602-610, 10.1080/02786820119445, 2001.

911   Wach, P., Spolnik, G., Rudzinski, K. J., Skotak, K., Claeys, M., Danikiewicz, W., and

912   Szmigielski, R.: Radical oxidation of methyl vinyl ketone and methacrolein in

913   aqueous droplets: Characterization of organosulfates and atmospheric

914   implications, Chemosphere, 214, 1-9, 10.1016/j.chemosphere.2018.09.026,

915   2019.

916   Wang, Y., Ren, J., Huang, X. H. H., Tong, R., and Yu, J. Z.: Synthesis of Four

917   Monoterpene-Derived Organosulfates and Their Quantification in Atmospheric

918   Aerosol Samples, Environ. Sci. Technol., 51, 6791-6801,

919   10.1021/acs.est.7b01179, 2017.

920   Wang, Y., Ma, Y., Kuang, B., Lin, P., Liang, Y., Huang, C., and Yu, J. Z.: Abundance of

921   organosulfates derived from biogenic volatile organic compounds: Seasonal and

922   spatial contrasts at four sites in China, Sci. Total. Environ., 806, 151275,

923   10.1016/j.scitotenv.2021.151275, 2022.

924   Wang, Y., Zhao, Y., Wang, Y., Yu, J. Z., Shao, J., Liu, P., Zhu, W., Cheng, Z., Li, Z., Yan,

925   N., and Xiao, H.: Organosulfates in atmospheric aerosols in Shanghai, China:

926   seasonal and interannual variability, origin, and formation mechanisms, Atmos.

927   Chem. Phys., 21, 2959-2980, 10.5194/acp-21-2959-2021, 2021.

928   Wang, Y., Hu, M., Wang, Y.-C., Li, X., Fang, X., Tang, R., Lu, S., Wu, Y., Guo, S., Wu,

929   Z., Hallquist, M., and Yu, J. Z.: Comparative Study of Particulate

930   Organosulfates in Contrasting Atmospheric Environments: Field Evidence for

931   the Significant Influence of Anthropogenic Sulfate and NOx, Environ. Sci.

932   Technol.Lett., 7, 787-794, 10.1021/acs.estlett.0c00550, 2020.

933   Wang, Y., Hu, M., Guo, S., Wang, Y., Zheng, J., Yang, Y., Zhu, W., Tang, R., Li, X., Liu,

934   Y., Le Breton, M., Du, Z., Shang, D., Wu, Y., Wu, Z., Song, Y., Lou, S., Hallquist,

935   M., and Yu, J.: The secondary formation of organosulfates under interactions

936   between biogenic emissions and anthropogenic pollutants in summer in Beijing,

937   Atmos. Chem. Phys., 18, 10693-10713, 10.5194/acp-18-10693-2018, 2018.

938   Xu, Y., Miyazaki, Y., Tachibana, E., Sato, K., Ramasamy, S., Mochizuki, T., Sadanaga,

939   Y., Nakashima, Y., Sakamoto, Y., Matsuda, K., and Kajii, Y.: Aerosol Liquid

940   Water Promotes the Formation of Water-Soluble Organic Nitrogen in

941   Submicrometer Aerosols in a Suburban Forest, Environ. Sci. Technol., 54,

942   1406-1414, 10.1021/acs.est.9b05849, 2020.

943   Yassine, M. M., Dabek-Zlotorzynska, E., Harir, M., and Schmitt-Kopplin, P.:

944   Identification of weak and strong organic acids in atmospheric aerosols by

945   capillary electrophoresis/mass spectrometry and ultra-high-resolution Fourier

946   transform ion cyclotron resonance mass spectrometry, Anal. Chem., 84, 6586-

947   6594, 10.1021/ac300798g, 2012.

948   Ye, J., Abbatt, J. P. D., and Chan, A. W. H.: Novel pathway of SO2 oxidation in the

949   atmosphere:reactions with monoterpene ozonolysis intermediates and

950   secondary organic aerosol, Atmos. Chem. Phys., 18, 5549-5565, 10.5194/acp-
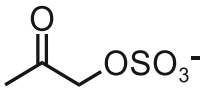
951   18-5549-2018, 2018.

952

953

954

955
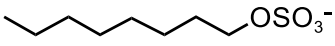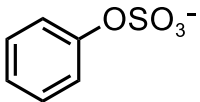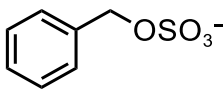
956

957
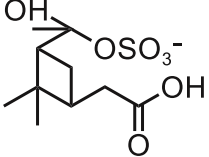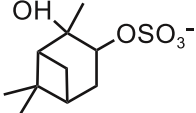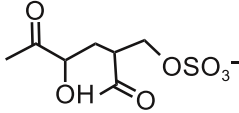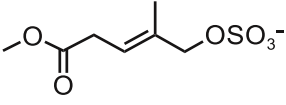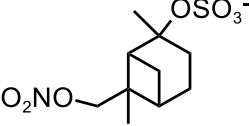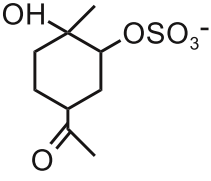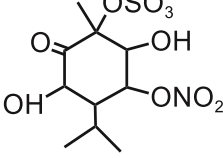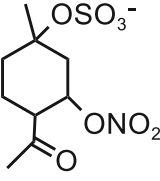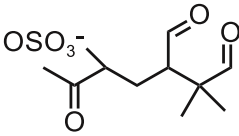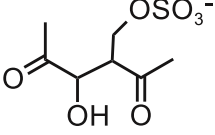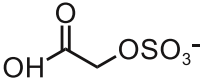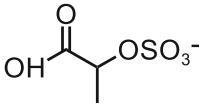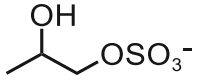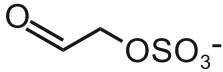
Table 1. Organosulfate quantification using UPLC-ESI(-)-QToFMS(/MS).

Formula[a]	MW (Da)	Standard	Structure	Reference
Isoprene-derived OSs (n = 12)				
$C_4H_7O_7S^-$	198.9912	Lactic acid sulfate (LAS)		(Hettiyadura et al. 2015)
$C_5H_{11}O_6S^-$	199.0276	LAS		(Riva et al. 2016a)
$C_5H_9O_7S^-$	213.0069	LAS		(Riva et al. 2016a)
$C_4H_7O_5S^-$	167.0014	LAS		(Schindelka et al. 2013)
$C_4H_7O_6S^-$	182.9963	LAS		(Shalamzari 2013)
$C_5H_7O_7S^-$	210.9912	LAS		(Hettiyadura et al. 2015)
$C_5H_9O_6S^-$	197.0120	LAS		(Riva et al. 2016a)
$C_5H_{10}NO_9S^-$	260.0076	LAS		(Surratt et al. 2007a)
$C_7H_9O_7S^-$	237.0069	LAS		(Nozière et al. 2010)
$C_5H_8NO_{10}S^-$	273.9869	LAS		(Nestorowicz et al. 2018)
$C_5H_{10}NO_9S^-$	260.0076	LAS		(Surratt et al. 2007a)
$C_5H_{11}O_7S^-$	215.0225	LAS		(Surratt et al. 2010)

Other quantified isoprene-derived OSs were shown in **SI**

Monoterpene-derived OSs (n = 10)

$C_{10}H_{17}O_7S^-$	281.0695	α-Pinene sulfate		(Nozière et al. 2010)
$C_{10}H_{17}O_5S^-$	249.0797	α-Pinene sulfate		(Wang et al. 2017)
$C_8H_{13}O_7S^-$	253.0382	Glycolic acid sulfate (GAS)		(Schindelka et al. 2013)
$C_7H_{11}O_6S^-$	223.0276	GAS		(Yassine et al. 2012)
$C_{10}H_{16}NO_7S^-$	294.0647	α-Pinene sulfate		(Surratt et al. 2008)
$C_9H_{15}O_6S^-$	251.0589	Limonaketone sulfate		(Wang et al. 2017)
$C_{10}H_{16}NO_{10}S^-$	342.0495	Limonaketone sulfate		(Yassine et al. 2012)
$C_9H_{14}NO_8S^-$	296.0440	Limonaketone sulfate		(Surratt et al. 2008)
$C_{10}H_{15}O_7S^-$	279.0538	GAS		(Surratt et al. 2007a)
$C_7H_{11}O_7S^-$	239.0225	GAS		(Nozière et al. 2010)

Other quantified monoterpene-derived OSs were shown in **SI**

C₂-C₃ OSs (*n* = 6)

$C_3H_5O_4S^-$	136.9909	GAS	unknown	(Yassine et
$C_2H_3O_6S^-$	154.9650	GAS		(Olson et al. 2011)

Formula	m/z	Name/Type	Structure	Reference
$C_3H_5O_6S^-$	168.9807	LAS	(structure)	(Olson et al. 2011)
$C_3H_7O_5S^-$	155.0014	GAS	(structure)	(Hettiyadura et al. 2019)
$C_2H_3O_5S^-$	138.9701	GAS	(structure)	(Yassine et al. 2012)
$C_3H_5O_5S^-$	152.9858	GAS	(structure)	(Hettiyadura et al. 2015)

OSa (aliphatic-OSs) (n = 1)

Formula	m/z	Name/Type	Structure	Reference
$C_8H_{17}O_4S^-$	210.0926	Sodium octyl Sulfate (SOS)	(structure)	(Wang et al. 2021)

Other quantified aliphatic-derived OSs were shown in **SI**

OSa (aromatic-OSs) (n = 2)

Formula	m/z	Name/Type	Structure	Reference
$C_6H_5O_4S^-$	172.9909	Phenyl sulfate	(structure)	(Wang et al. 2021)
$C_7H_7SO_4S^-$	218.9786	Phenyl sulfate	(structure)	(Wang et al. 2021)

Other quantified aromatic-derived OSs were shown in **SI**

OS$_a$-other (n =3)

Formula	m/z	Name/Type	Structure	Reference
$C_4H_7O_4S^-$	151.0065	Methyl sulfate	unknown	(Wang et al. 2021)
$C_5H_7O_6S^-$	194.9963	GAS	unknown	(Wang et al. 2021)
$C_6H_9O_6S^-$	209.0120	GAS	unknown	(Berndt et al. 2016)

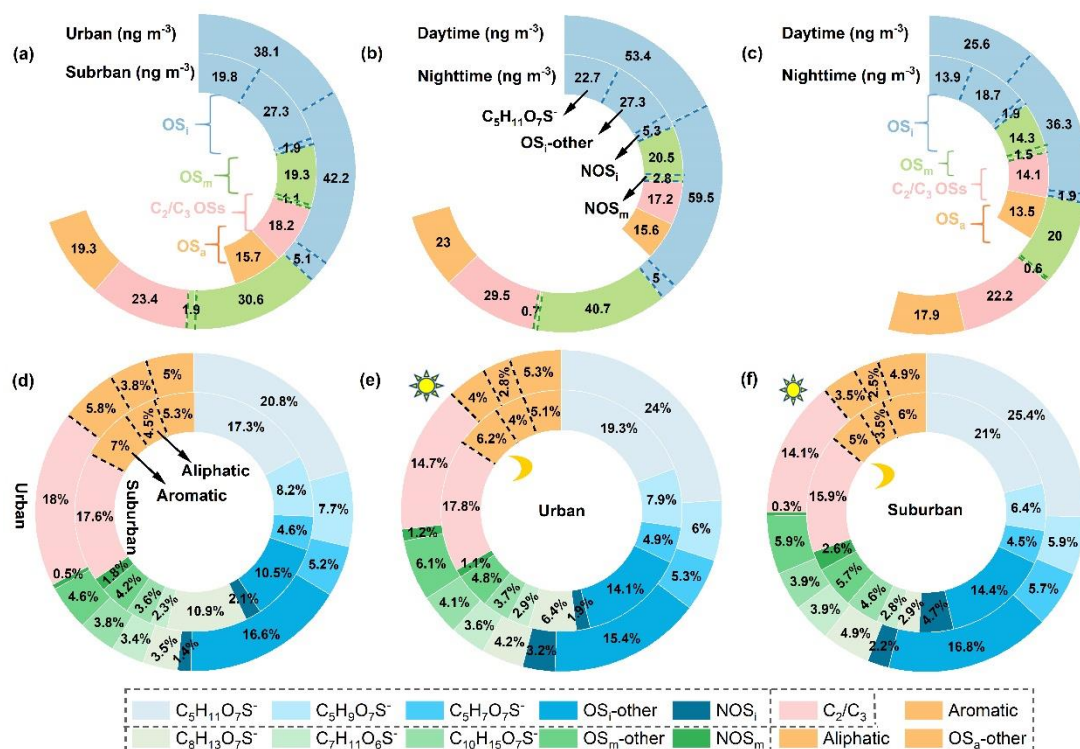959 [a] MS/MS data supports tentative structural identification based on the listed references.

960

961

962

963

964

965

966

967 **Figure 1.**

Figure 1. Average distributions in the mass concentrations and mass fractions of various OSs in PM$_{2.5}$ in different cases: (a–d) urban vs suburban for all data, (b–e) daytime vs nighttime in the urban area, as well as (c–f) daytime vs nighttime in the suburban area. The areas divided by dashed lines in Figures a-c indicate C$_5$H$_{11}$O$_7$S$^-$, OS$_{i\text{-other}}$, NOS$_i$, and NOS$_m$ in sequence, as illustrated in Figure b. The areas divided by dashed lines in Figures d-f indicate aromatic and aliphatic OSs in sequence, as illustrated in Figure d.
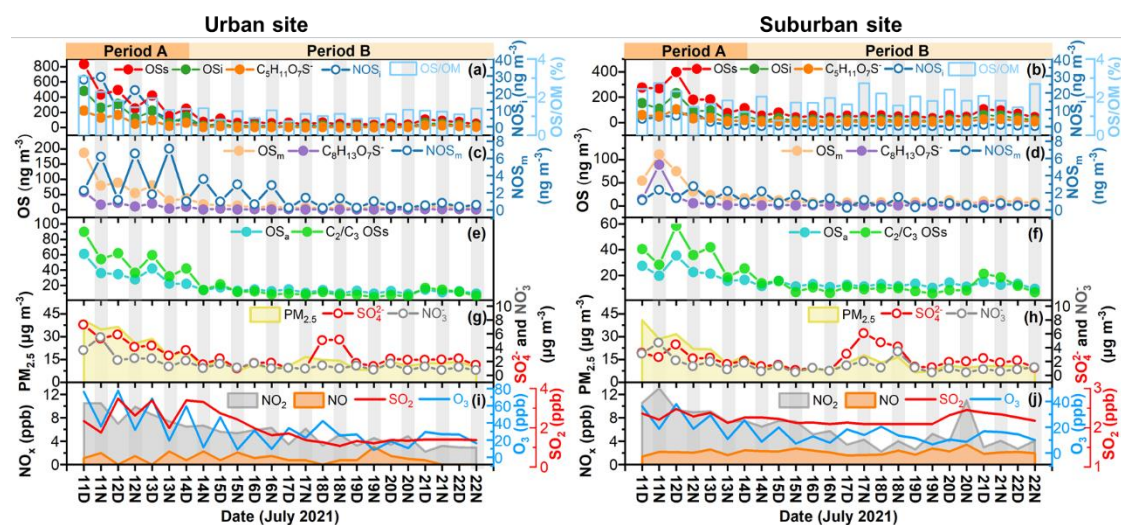
Figure 2.

Figure 2. Temporal variations of OSs and other chemical components in $PM_{2.5}$ as well as other data measured in urban and suburban Shanghai in summer. (a–b) OSs, OS_i, $C_5H_{11}O_7S^-$ (major OS_i species), NOS_i, and OS/OM (%); (c–d) OS_m, $C_8H_{13}O_7S^-$, and NOS_m; (e–f) OS_a and C_2-C_3 OSs; (g–h) $PM_{2.5}$, SO_4^{2-}, and NO_3^-; and (i–j) NO_2, NO, SO_2, and O_3. The sampling period A and B indicate the relatively polluted period and the clean period, respectively.

988 **Figure 3.**

989
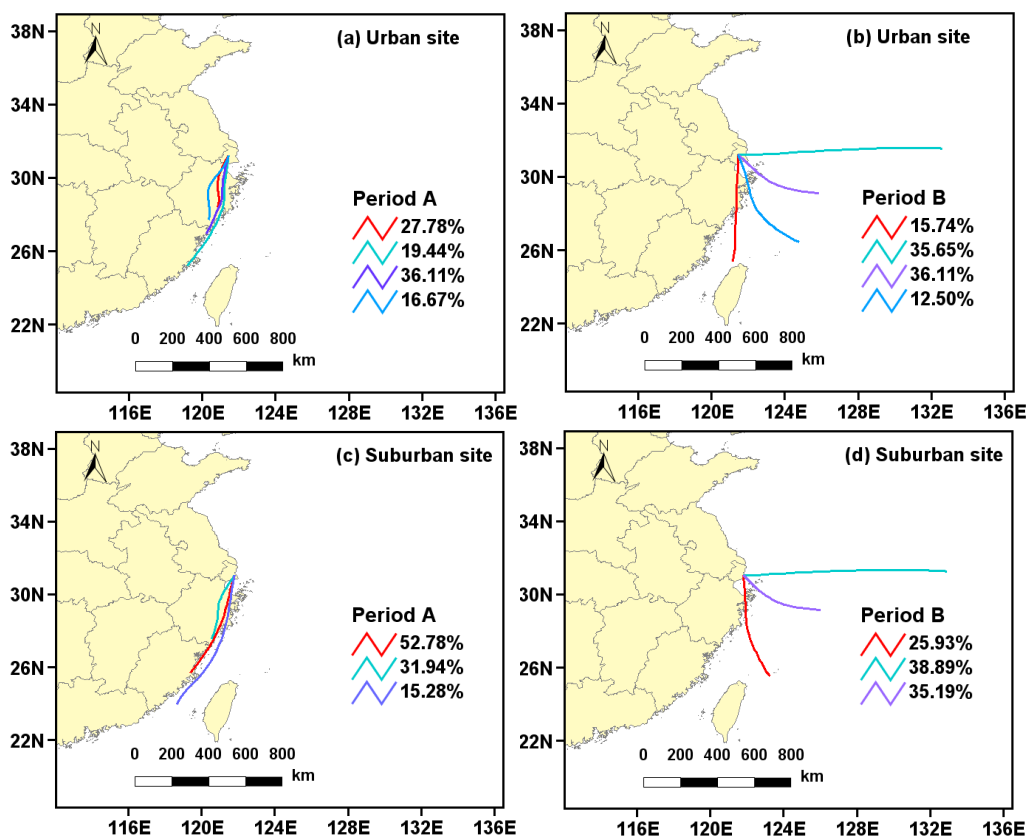
990
991

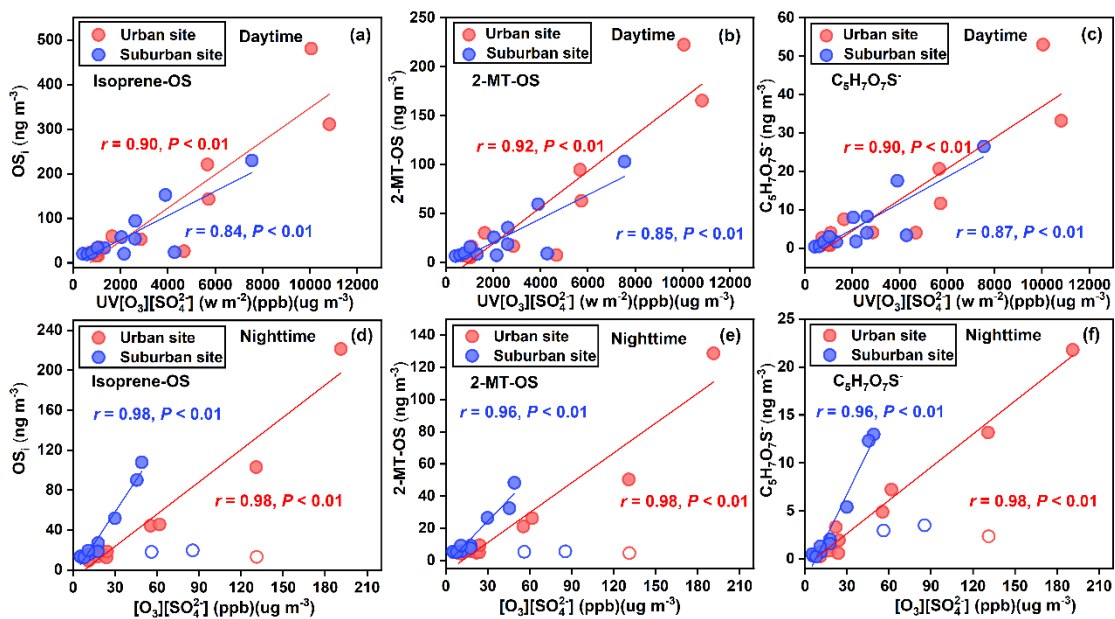992 **Figure 3.** Air mass backward trajectories of the major clusters in different periods in

993 the (a–b) urban and (c–d) suburban areas.

994
995

Figure 4.

997

998

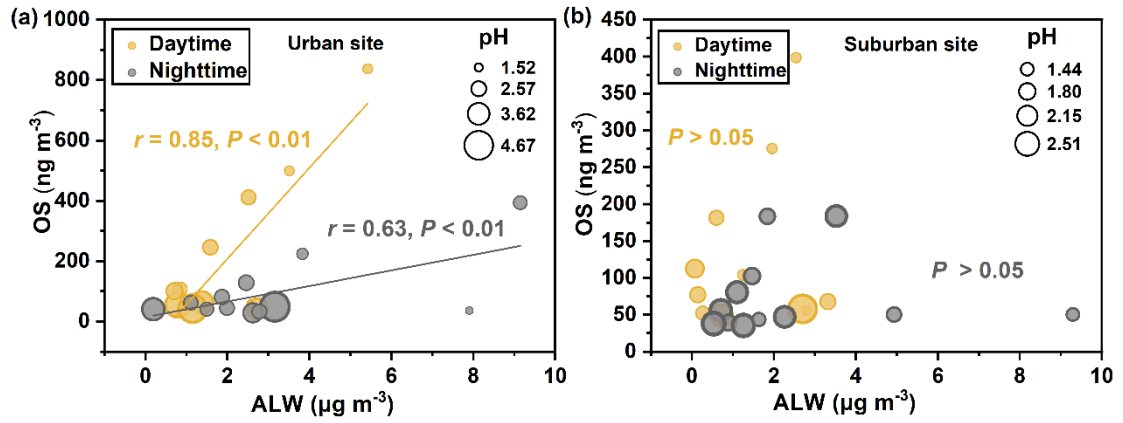**Figure 4.** Mass concentrations of (a and d) OS_i, (b and e) 2-MT-OS, and (c and f) $C_5H_7O_7S^-$ as functions of $UV[O_3][SO_4^{2-}]$ and $[O_3][SO_4^{2-}]$ during daytime and nighttime in the urban (red solid circles) and suburban sites (blue solid circles). The open circles represent outliers, which was attributed to several particularly high sulfate events.
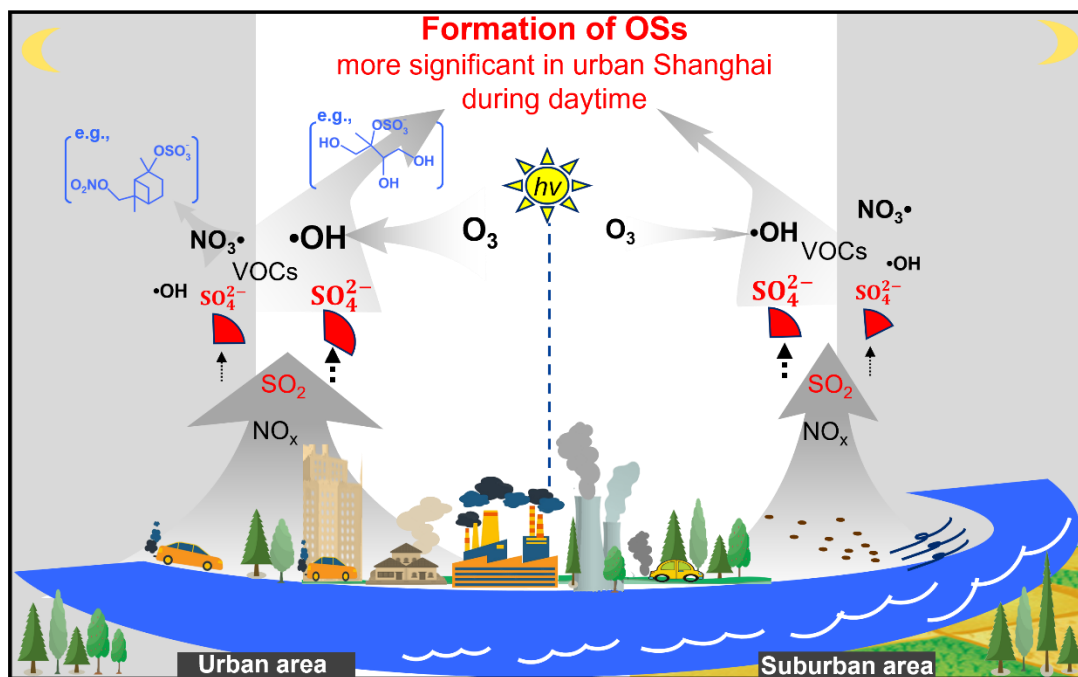
1003

Figure 5.

Figure 5. Scatterplots of the ALW concentrations with the mass concentrations of total

OSs in $PM_{2.5}$ collected in the (a) urban and (b) suburban areas. Yellow and grey lines

show regression lines in the daytime and nighttime, respectively.

Figure 6. Conceptual picture showing the characteristic and atmospheric process of OSs in urban and suburban Shanghai.